

Direct Imaging of Exoplanets and Brown Dwarfs with the VLT: NACO Pupil-stabilised Lyot Coronagraphy at 4 μm

Markus Kasper¹
 Paola Amico¹
 Emanuela Pompei¹
 Nancy Ageorges²
 Daniel Apai³
 Javier Argomedo¹
 Nick Kornweibel¹
 Chris Lidman¹

¹ ESO

² Max-Planck-Institut für extraterrestrische Physik, Garching, Germany

³ Space Telescope Science Institute, Baltimore, USA

NACO is the versatile adaptive optics assisted near-infrared instrument at the VLT. Among its many modes it offers spectral differential imaging that efficiently enhances the contrast in searches for faint companions. Recently, an additional method to calibrate quasi-static speckles through angular differential imaging has been developed, offering the option to operate NACO in a pupil-tracking mode. Using this new mode, in combination with Lyot coronagraphy and an optimal choice of observing wavelength in the thermal infrared around 4 μm , allows NACO to reach unprecedented sensitivities for masses of companions for all but the hottest exoplanets, beginning to open up the mass domain targeted by future instruments such as SPHERE.

For about half a decade surveys for planetary-mass companions have been carried out in the near-infrared (near-IR) by three methods: broadband imaging (e.g., Chauvin et al., 2003; Masciadri et al., 2005); spectral differential techniques in narrowband filters inside and outside the H -band, using the methane absorption features to subtract speckle noise efficiently (called spectral differential imaging [SDI]; see, for example, Biller et al., 2007); and using angular differential imaging techniques (ADI; see Lafrenière et al., 2007). In addition, specialised instruments (e.g., NIRC2 at Gemini South and HiCiao at Subaru) that even combine H -band SDI with ADI recently began operation and are expected to produce first results very soon. The improved understanding of the high-contrast imag-

Table 1. Possible planetary-mass companions discovered by direct imaging.

Object	Contrast (mag)	Separation (arcsec.)	Discovery instrument and reference
2M1207 b	$\Delta J = 7$ $\Delta H = 5.7$ $\Delta K = 5$ $\Delta L = 3.6$	0.77	NACO Broadband (Chauvin et al., 2005)
GQ Lup b	$\Delta H = 6$ $\Delta K = 6.2$ $\Delta L = 5.8$	0.73	NACO Broadband (Neuhäuser et al., 2005)
Beta Pic b	$\Delta L = 7.7$	0.41	NACO L' (Lagrange et al., 2009)
HR 8799 b	$\Delta J = 13.9$ $\Delta H = 12.6$ $\Delta K = 11.8$ $\Delta L = 10.5$	1.73	Keck NIRC2/Gemini NIRC2 Broadband, ADI (Marois et al., 2008)
HR 8799 c	$\Delta J = 12.2$ $\Delta H = 11.6$ $\Delta K = 10.9$ $\Delta L = 9.5$	0.95	Keck NIRC2/Gemini NIRC2 (Marois et al., 2008)
HR 8799 d	$\Delta J = 12.9$ $\Delta H = 11.6$ $\Delta K = 10.9$ $\Delta L = 9.4$	0.63	Keck NIRC2/Gemini NIRC2 (Marois et al., 2008)

ing problem and corresponding improvements in ground-based instrumentation and observing strategies have recently led to the first direct images of planetary-mass companions around the early-type (around A5) stars HR8799 (Marois et al., 2008) and Beta Pic (Lagrange et al., 2009). Table 1 lists possible planetary-mass companions discovered by ground-based direct imaging, together with their separation and the contrast in magnitudes to their host stars in various bands.

The advantages of the thermal infrared, especially the long end of the L -band, have only recently been realised (e.g., Kasper et al., 2007; Janson et al., 2008). This wavelength range offers considerable advantages compared to shorter wavelengths, the most important one being the improved contrast of planetary-mass companions with respect to their host stars. Models predict $H-L$ colours of around 2 mag for a 1000 K companion (a 5 Jupiter mass [M_J] object at an age of 30 Myr or a 30 M_J object at 1 Gyr) and an $H-L$ colour ~ 4.5 mag for a 350 K companion (1 M_J at 30 Myr or 5 M_J at 1 Gyr). Obviously, the L -band offers tremendous gains for observing lower mass and older objects. As an example, the planetary-mass companion to the brown dwarf 2M1207, or the companions of HR 8799 (see Table 1), have an L -band contrast with respect to their host stars which is about 2 magnitudes more favourable than in the H -band! An additional advan-

tage of adaptive optics (AO) assisted L -band over shorter wavelength observations is the better and more stable image quality, with Strehl ratios well above 70%, and sometimes as high as 85%, thus reducing speckle noise and facilitating point spread function (PSF) subtraction. All these advantages more than compensate for the increased sky background in the thermal infrared.

In the following, we describe the science requirements for high-contrast imaging and the technical tests that were carried out with NACO in pupil-tracking mode using the NB4.05 filter with and without the 0.7-arcsecond diameter stop of the Lyot coronagraph. This combination of NACO instrument settings (Pupil Stabilised Coronagraphy at 4 μm , hereafter denoted PSC4Mu) is identified as the currently most sensitive mode for planetary-mass companion detection in the close vicinity of bright stars, worldwide. Using it, NACO is even sensitive to mass regimes similar to the ones that will be become accessible with SPHERE, albeit at larger orbital separations. Hence, NACO PSC4Mu will be able to nicely complement detections with SPHERE in the thermal IR.

Science requirements

Burrows et al. (2003) explored the spectral and atmospheric properties of brown

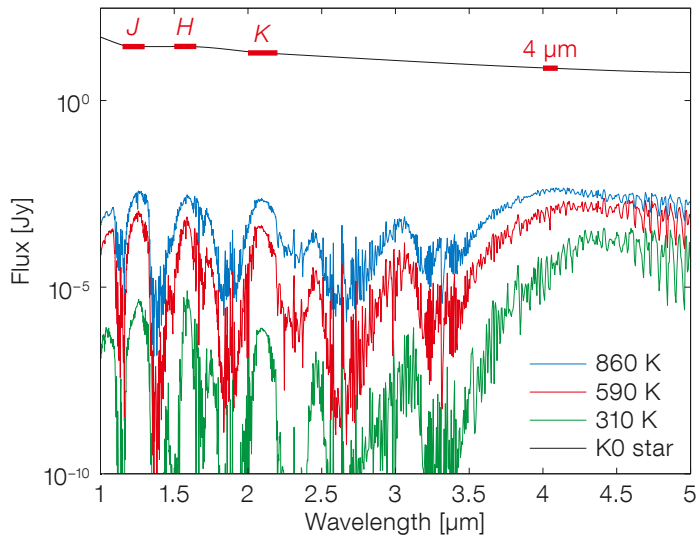


Figure 1. Absolute flux density of giant exoplanets in the near- to mid-IR. For reference, the black lines indicate the flux of a K0 star located at 10 pc in several filters (see Table 2).

Filter	λ_1 [μm]	λ_2 [μm]
J	1.20	1.25
H	1.55	1.60
K	2.05	2.15
L'	3.50	4.10
4 μm	4.0	4.10

Table 2. Filter widths assumed for the contrast analysis. The filters are assumed to transmit all radiation between limits λ_1 and λ_2 and block it completely outside these limits.

dwarfs cooler than the latest known T dwarfs. Their focus was on the yet-to-be-discovered free-floating brown dwarfs in the T_{eff} range from ~ 800 to ~ 130 K and with masses from 25 to $1 M_J$. Evolutionary models were used to determine T_{eff} as a function of age and mass, and atmospheric models were used to calculate the resulting spectra. Burrows et al. (2003) concluded that studies in the mid-infrared could assume a new, perhaps transformational, importance in the understanding of the coolest brown dwarfs and giant exoplanets. The modelled spectral energy distributions (SEDs) provided by Burrows were used for the analysis and conversion between point spread function contrast and detectable planet mass.

Since the radius of a giant planet rapidly converges to around 1 Jupiter radius (R_J) and surface gravity effects play only a minor role, the planet's spectrum is primarily determined by the planet's effective temperature, which is a function of its mass and age. Figure 1 shows the absolute flux of giant exoplanets in the near- to mid-IR for different effective temperatures. The red lines indicate the flux of a K0 star located at 10 parsecs (pc) in several filters for reference. The non-blackbody SED with pronounced absorption in the H_2O , CH_4 and NH_3 molecular bands is striking. It is also apparent from this figure that the flux contrast between star and planet at $4 \mu\text{m}$ is greater than in the near-IR, hence this wavelength is more favourable for planet detection. This con-

trast advantage increases towards lower effective temperatures and thus toward older and lower mass planets.

Based on these simulated spectra, the contrasts were calculated for the spectral regions/filters listed in Table 2. For each near-IR band, the regions with the most favourable possible contrasts (unaffected by molecular absorption) are used in the comparisons. While the planet/star contrast ratio is fairly similar in the near-IR (J, H, K) for all values of T_{eff} , it is clear that the contrast at $4 \mu\text{m}$ is always superior to that in the near-IR by factors between ~ 5 (at 800 K) and ~ 50 (at 300 K), as evident from Figure 2.

The price to be paid when observing in the thermal IR is the reduced sensitivity because of the increased sky background. On Paranal, for example, the typical instrumental background (sky + telescope)¹ in the H-band is 14.4 mag arcsecond⁻², while the background in L-band is 3.9 mag arcsecond⁻². Using the NACO exposure time calculator (ETC), background-limited 5σ detection of magnitude 16.3 point sources is possible in 2 hours using the NB4.05 filter (i.e. the red end of L' filter, which is best for exoplanet detection), while in the same time in the NB1.64 filter (H-band, SDI-like filter width), sources as faint as 21.7 mag can be detected. As shown in Figure 3, H-band and $4 \mu\text{m}$ filters have a similar background-limited sensitivity for ~ 300 K objects, while the H-band is more sensitive for warmer objects (i.e. the H- $4 \mu\text{m}$ colour varies between 4.5 for $T_{\text{eff}} = 300$ K and 2 for $T_{\text{eff}} = 850$ K). Objects with temperatures around 300 K would be detectable in both filters up to about 10 pc distance (the absolute magnitude is similar to the background-limited detectivity), while a 600 K planet would be detected up to a distance modulus of ~ 3 mag or 40 pc at $4 \mu\text{m}$ and up to a distance modulus of 5.7 or 140 pc in

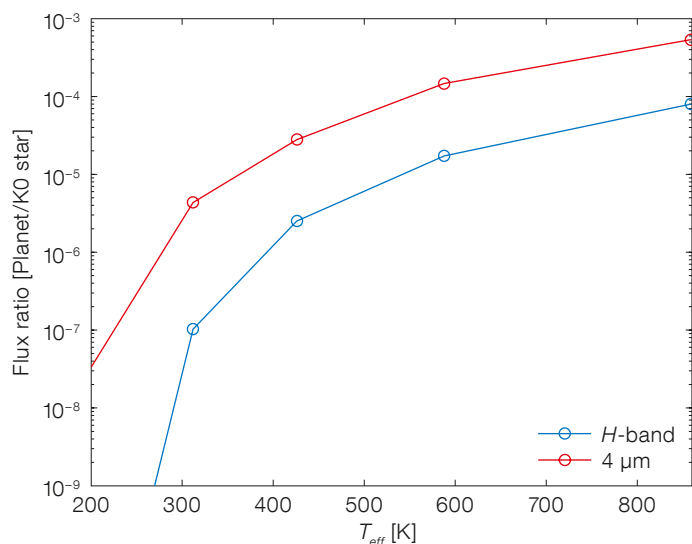


Figure 2. Contrast ratio of a planet to host K0 star as a function of the planet's effective temperature for H-band, shortwards of the CH_4 absorption (in blue) and $4 \mu\text{m}$ observations (in red).

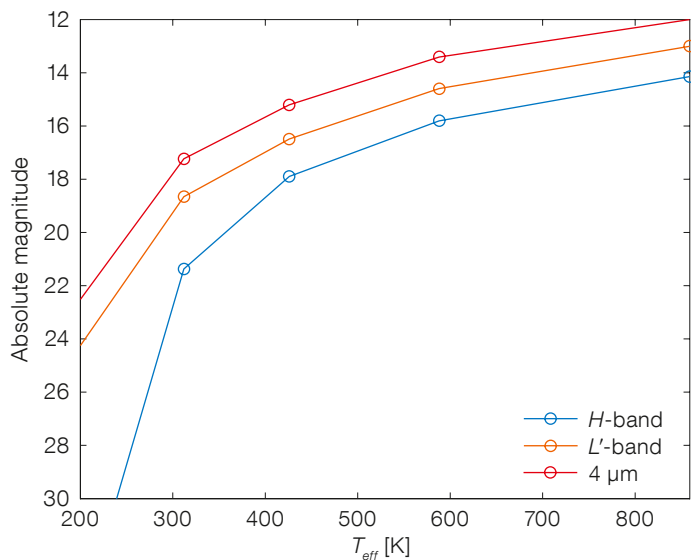


Figure 3. Absolute magnitudes of exoplanets in different filters as a function of effective temperature in the H , L' and 4 μm bands.

H -band. Thus, isolated warm planets are more easily detected in the near-IR because of the lower sky background. Figure 3 also shows the absolute magnitude of exoplanets in L' to demonstrate the 1–1.5 magnitude advantage of the 4 μm filter. The 4 μm filter is at a favourable wavelength to cover just the peak of the spectrum (see Figure 1), while the shorter end of L' does not capture much flux from an exoplanet.

NACO pupil-stabilised imaging at 4 μm

One of the main impediments to reaching the highest contrasts is the presence of quasi-static speckles that cannot easily be distinguished from a faint companion in a long-exposure image. These quasi-static speckles are created by imperfections or aberrations of the telescope and instrument optics and persist over time spans covering an observation. Hence, their intensity integrates in the same way as the exoplanet's flux and no improvement of contrast signal-to-noise ratio (SNR) in an ordinary image can be obtained with increase in the observing time.

However, efficient methods exist to calibrate quasi-static speckles and to improve contrast. SDI exploits the fact that speckles show spectral features of the star, while a reasonably cool exoplanet shows strong molecular bands that allow

it to virtually disappear at certain wavelengths. Subtracting an image taken inside the molecular band from one taken in the adjacent continuum leaves the image of the planet, while removing the speckles. ADI is another method that can be used if the field of view, and hence the image of the exoplanet, is allowed to rotate with respect to the telescope/instrument configuration and hence the quasi-static speckle pattern. The difference between two images with relative field of view rotation would efficiently remove quasi-static speckles, while leaving the exoplanet (provided that the rotation is large enough to avoid overlap between the exoplanet's images at the desired angular separation). ADI is rather simple to implement for non-rotating instruments mounted at the Cassegrain focus of an alt-azimuth telescope, because only the field would rotate with the parallactic angle. The situation at the Nasmyth focus (where NACO is mounted) is more complex, since a stationary instrument would see both pupil and field rotating during observations. NACO is mounted instead on the adaptor-rotator that itself rotates the whole instrument in order to keep the field orientation fixed. An alternative rotation mode called pupil-tracking has recently been implemented to allow NACO to rotate with the pupil, effectively freezing the telescope/instrument relative orientation and hence the quasi-static speckle pattern. In this mode, the instrument field of view again rotates

with the parallactic angle and true ADI is possible.

While SDI relies on a “known” spectrum of quasi-static speckles, ADI relies on temporally static aberrations. This is a strong assumption, especially because NACO still de-rotates the pupil with telescope altitude and so may experience significant variations of the gravity vector, leading to instrument flexure during an observation. ADI is most effective when observing an object passing through the meridian, because pupil rotation rate is a minimum while field $v.$ pupil rotation rate is a maximum there.

The efficiency of the pupil-tracking mode of NACO was tested on a bright star close to the meridian in favourable DIMM seeing of 0.6–0.7 arcseconds. The AO performance with the 14 \times 14 lenslet array was very good, delivering Strehl ratios higher than 80 % in the NB4.05 filter. While the fixed position of the pupil is demonstrated by the well-defined, un-smearred diffraction of the telescope spider arms, the parallactic angle changed and hence the field of view (FoV) rotated by almost 70 degrees over the 30-minute observation.

Individual 30-second exposures (DIT 0.2s, NDI 150) were recorded on a dither pattern that allowed us to remove the sky background. Then the images were high-pass filtered to remove smooth PSF structures (atmospheric speckle halo) and increase the speckle contrast. Figure 4 shows a sequence of three 30-second exposures where the second image was taken 5 minutes and the third image 30 minutes after the first one. The speckle pattern shows a remarkable stability over a period of 30 minutes.

The rate of parallactic angle change is an important parameter for ADI image reduction. In order to avoid the overlap of a λ/D -sized object at 5 λ/D separation ($\lambda/D \sim 0.1$ arcseconds at 4 μm wavelength and the VLT), a minimum field rotation of 11.4° between two images is required. Typically, the rate of change of rotation for an object of declination -40° near the meridian observed from Paranal (latitude -24°) is of the order 0.015°/s. Hence, ADI reduction typically needs

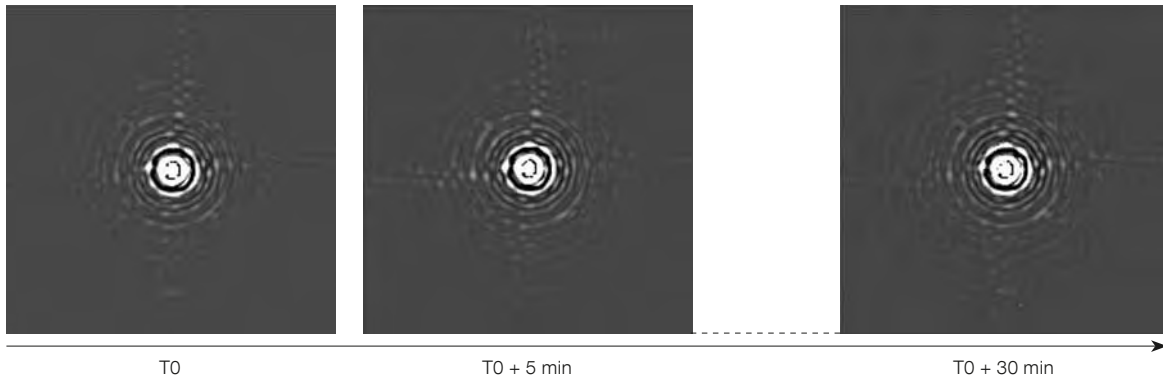


Figure 4. Sequence of three 30-second exposures in pupil-tracking mode, where the second was taken 5 minutes and the third 30 minutes after the first. The images were high-pass filtered to enhance the contrast of the speckle pattern.

image pairs separated by $11.4/0.015$ seconds or at least 10 minutes in time.

The ADI reduction of the individual 30-second exposures now consists of the following major steps:

i) Images separated in time as close as the parallactic angle change allows (criterion, for example, $> 11.4^\circ$) are re-centred and subtracted from each other. Here the normalisation can be quite difficult, since the intensity of the quasi-static speckle pattern scales with the AO-corrected Strehl ratio (better correction means stronger speckles!) and its determination is not always an easy task (e.g., when the stellar PSF core saturates the detector). Alternatively, one could also try to determine the normalisation factor that leads to minimum intensity in the subtracted image or in annuli of certain radii from the centre. Due to the stable seeing conditions and corresponding AO correction, no image normalisation was necessary here.

ii) The subtracted images are de-rotated by the parallactic angle offset to the first image of the pair and summed up.

The output of the ADI processing steps described above is given in Figure 5. For reference, artificial benchmark planets were inserted into the unprocessed data to verify the contrast levels calculated from the residual speckle pattern. Without a coronagraph, the PSF contrast of $4\text{-}\mu\text{m}$ ADI imaging beyond 0.5-arcsecond separation is already better than can be achieved with SDI, even without considering the additional contrast gain in planetary mass provided by the favourable planet-to-star contrast at $4\text{ }\mu\text{m}$ compared to the near-IR (Figure 2).

NACO pupil-stabilised coronagraphy at $4\text{ }\mu\text{m}$

Even further contrast improvements can be expected from coronagraphy. The reduction of the Airy pattern by a coronagraph brings two major benefits:

i) It reduces the so-called “pinned” speckles that result from interference between light from the speckle and from the Airy rings. Since the intensity of a pinned speckle is proportional to the Airy intensity, the small classical Lyot coronagraph of NACO (0.7 arcsecond diameter mask and a Lyot stop undersized to 90% of the pupil diameter) should reduce the intensity of pinned speckles by a factor of a few tens.

ii) It reduces the intensity of speckles originating from the optics after the coronagraphic mask (i.e. all optics inside CONICA) by the coronagraphic suppression of the PSF core, which is better than a factor of 100 in the case of the NACO small Lyot coronagraph.

To confirm the positive effect of the coronagraph, individual 1-minute exposures (DIT 1 s, NDIT 60) were recorded using NACO in pupil-tracking mode with the small Lyot coronagraph and the NB4.05 filter (PSC4Mu method), that will turn out to be most effective for exoplanet detection with NACO. One drawback of coronagraphy is that dithering is no longer possible and sky background has

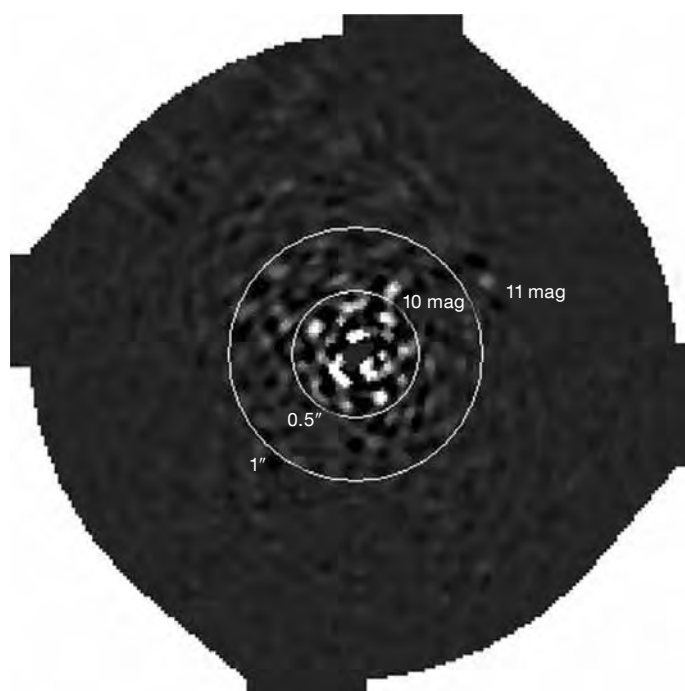


Figure 5. Final ADI processed non-coronagraphic image. Two artificial benchmark planets of delta magnitude 10 and 11, were inserted into the unprocessed data to verify the contrast level calculated from the residual speckle pattern.

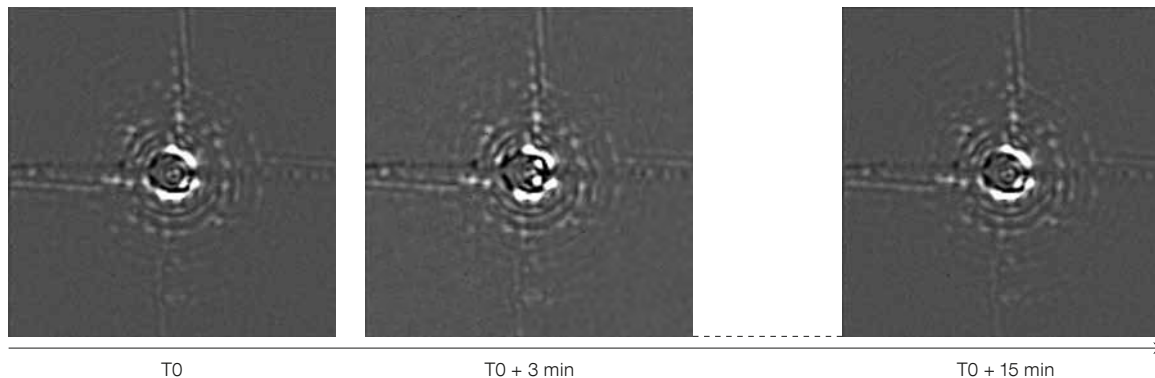


Figure 6. Sequence of three 1-minute exposures in pupil-tracking mode with coronagraphy, where the second was taken 3 minutes and the third 15 minutes after the first. The images were high-pass filtered to enhance the contrast of the speckle pattern.

to be recorded separately, thus decreasing the on-source efficiency. However, for small-field high-contrast imaging observations, the impact of a variable sky background mainly consists of constant offsets that can be removed very efficiently by the data reduction. Another complication is the movement of the star image relative to the coronagraphic mask (possibly introduced by an unstable mask position) that currently requires frequent manual adjustment of the star's position to keep it centred on the mask.

Figure 6 shows a sequence of three 1-minute exposures where the second image was taken 3 minutes and the third 15 minutes after the first image. Again, the speckle pattern shows a remarkable

stability over 15 minutes. In addition, the intensity of quasi-static speckles is dramatically reduced in comparison to the non-coronagraphic images (Figure 4) as expected.

Following similar ADI data reduction steps as described above for the non-coronagraphic imaging, the final image shown in Figure 7 results. The same two artificial planets have again been inserted and now appear at a much better contrast SNR. Actually planets that are even more than 11 magnitudes fainter than the central star could be detected, with sufficient confidence, at separations larger than about 0.5 arcseconds. For angular separations smaller than 0.5 arcseconds, the achievable contrast quickly deteriorates

and is worse than with non-coronagraphic imaging. At such separations, the impact of edge effects at the coronagraphic mask, which vary strongly with the precise centring of the star, dominate over residual speckle intensity and degrade the achieved contrast.

Residual radial contrast curves of the non-coronagraphic and the coronagraphic images after spatial filtering (SF) and ADI correction (Figure 5 and Figure 7) have been derived from the standard deviation of the intensity fluctuations in a 2 pixel-wide annulus centred on the star. The contrast was normalised to unit intensity of the peak of the non-coronagraphic image, and the reduced off-axis throughput of the coronagraph (90% undersized pupil stop) has been taken into account. Figure 8 shows the derived 1σ contrast as well as a theoretical Airy pattern and the profile of the non-coronagraphic PSF (saturated in the centre) with an estimated Strehl ratio of 85%. At 0.5 arcsecond separation, the ADI-reduced coronagraphic image achieves a 1σ contrast performance of about 7×10^{-6} . Assuming that 5σ is sufficient for a safe ADI detection, the achievable contrast at this separation is better than 11 magnitudes, as demonstrated by Figure 7. This mode of NACO is efficient enough to ensure that the contrast beyond 1 arcsecond is essentially limited by sky background, and therefore similar to an isolated object.

Using the exoplanet evolutionary and atmospheric models of Burrows et al. (2003) referred to earlier, the measured PSF contrast can be converted into an exoplanet mass sensitivity, assuming a given stellar brightness and age. Figure 9 shows the result of this analysis

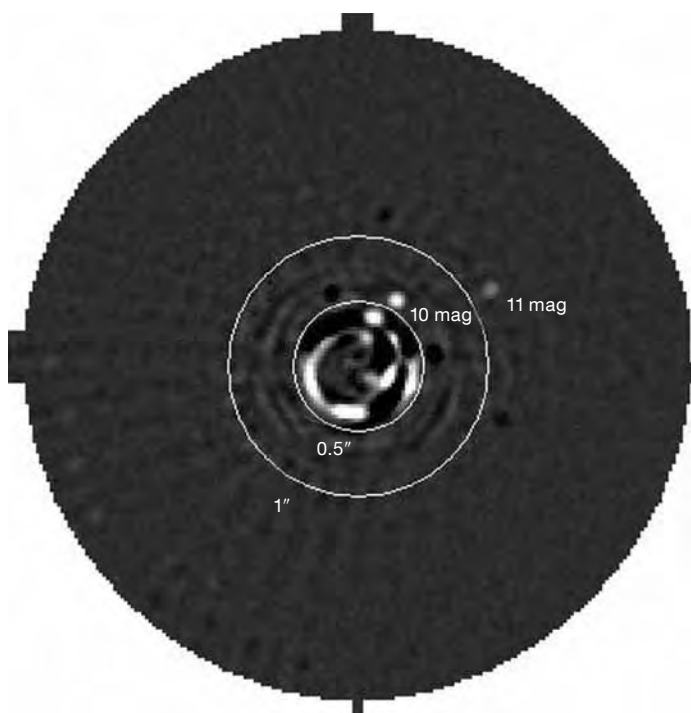


Figure 7. Final ADI processed coronagraphic image. Two artificial benchmark planets were inserted into the unprocessed data to verify the contrast levels calculated from the residual speckle pattern are indicated (c.f. Figure 5).

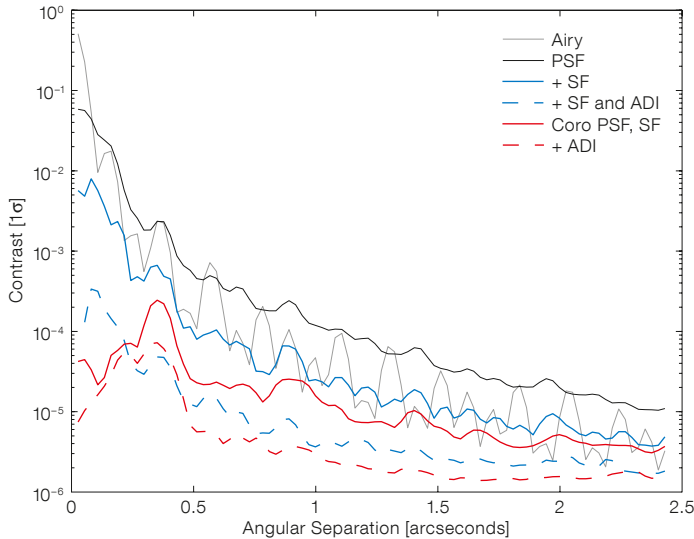


Figure 8. Contrasts measured on the non-coronagraphic (blue) and coronagraphic (red) images after different steps of the data reduction (spatial high-pass filter – SF and ADI).

same factor of five and a much greater efficiency in direct imaging of giant exoplanets would be reached.

References

Biller, B. et al. 2007, ApJS, 173, 143
 Burrows, A., Sudarsky, D. & Lunine, J. I. 2003, ApJ, 596, 587
 Chauvin, G. et al. 2003, A&A, 404, 157
 Chauvin, G. et al. 2005, A&A, 438, L25
 Chun, M. et al. 2008, Proc. SPIE, 7015, 49
 Janson, M. et al. 2008, A&A, 488, 771
 Kasper, M. et al. 2007, A&A, 472, 321
 Lafrenière, D. et al. 2007, ApJ, 670, 1367
 Lagrange, A.-M. et al. 2009, A&A, 493, 21
 Masciadri, E. et al. 2005, ApJ, 625, 1004
 Marois, C. et al. 2008, Science, 322, 1348
 Neuhauser, R. et al. 2005, A&A, 435, L13

Links

¹ <http://www.eso.org/gen-fac/pubs/astclim/paranal/skybackground/>

assuming a K0 type star and ages of 100 and 316 Myr. For comparison, the same analysis was carried out with the best SDI contrasts reported by Biller et al. (2007) and the NICI contrast obtained during commissioning (Chun et al., 2008). While NACO–SDI contrast appears to lag behind, it must be noted that SDI could also benefit from coronagraphy and pupil-tracking; a quantitative evaluation of such an observing strategy remains to be done.

Pupil-stabilised coronagraphy at 4 μ m is a very sensitive observing method for detection for all but the hottest exo-

planets, delivering unprecedented mass contrasts. Excitingly, this mode of NACO already begins to open up the mass domain targeted by future instruments, such as SPHERE. However, the background-limited point-source sensitivity in the thermal IR makes it optimal for relatively nearby targets with distances up to a few tens of pc. The advantage of the method could be extended even further by installing a new astronomical filter in CONICA that would increase the bandwidth by about a factor of five over the one provided by the currently installed NB4.05 filter. With such a new filter the observing times required would be reduced by the

Figure 9. Detectability expressed in planet mass (assuming K0 host star) of the NACO PSC4Mu mode, compared to NACO SDI and GEMINI NICI using modelled exoplanet spectra for 100 Myr age (left) and 316 Myr age (right). A 3 σ detection criterion was used for all instrument contrasts.

